A Weak Antiferromagnetic Interaction between Mn^{2+} Centers through a TCNQ Column: Crystal Structures and Magnetic Properties of $[Mn^{II}(tpa)(TCNQ)(CH_3OH)](TCNQ)_2 \cdot CH_3CN$, $[Mn^{II}(tpa)(\mu\text{-}O_2CCH_3)]_2(TCNQ)_2 \cdot 2CH_3CN$, and $[Mn^{II}(tpa)(NCS)_2] \cdot CH_3CN$ (tpa = Tris(2-pyridylmethyl)amine)

Hiroki Oshio,*,† Etsuo Ino,† Iwao Mogi,‡ and Tasuku Ito*,†

Department of Chemistry, Faculty of Science, Tohoku University, Aoba-ku, Sendai 980, Japan, and Institute for Materials Research, Tohoku University, Aoba-ku, Sendai 980, Japan

Received July 8, 1993®

Reaction of $Mn(CH_3COO)_2 \cdot 4H_2O$ and $Mn(PF_6)_2 \cdot 4H_2O$ with tpa and Li(TCNQ) (tpa = tris(2-pyridylmethyl)-amine, TCNQ = tetracyanoquinodimethane) in acetonitrile–methanol solution gave $[Mn^{II}(tpa)(\mu\text{-}O_2CCH_3)]_2(TCNQ)_2 \cdot 2CH_3CN$ (**1**) and $[Mn^{II}(tpa)(TCNQ)(CH_3OH)](TCNQ)_2 \cdot CH_3CN$ (**2**), respectively. Crystal structures and magnetic properties have been studied in comparison with those of $[Mn^{II}(tpa)(NCS)_2] \cdot CH_3CN$ (**3**). Complex **1** crystallizes with an inversion center located in the center of the bis(μ-acetato)dimanganese(II) core, and TCNQ units form diamagnetic dimers which stack to form a column structure. The acetates bridge the two Mn(II) centers in a syn–anti mode, with a Mn–Mn separation of 4.145(1) Å, and mediate a weak antiferromagnetic interaction with $J = -0.972(6)$ cm^{-1} (where $H = -2JS_1 \cdot S_2$). In **2**, four crystallographically independent TCNQ ions, called **A**, **B**, C, and **D**, respectively, were revealed in the unit cell, and anions **C** and **D** are located on the crystallographic inversion center. Anions **A** and **B** form dimeric units (**AA** and **BB**), respectively, and these dimers respectively stack with **C** and **D** to form columns (···**AACAA**···) and (···**BBDBB**···). The $[Mn^{II}(tpa)(CH_3OH)]$ unit was directly bound by the anion **B**, and as a result, two manganese atoms were connected through two **B** anions with a Mn–Mn separation of 15.397(2) Å. The temperature dependence of the magnetic susceptibility of **2** has shown an antiferromagnetic behavior; that is, $\chi_m T$ values start to gradually decrease from 4.4 emu K mol^{-1} at 100 K to 1.76 emu K mol^{-1} at 2 K. In **3**, a manganese ion has a six-coordinate geometry, which is similar to that of **2**, and the closest Mn–Mn separation is 6.8873(9) Å. Magnetic susceptibility measurement for **3** has revealed the Curie behavior down to 4 K and this leads one to conclude that zero-field splitting for the manganese ion and an antiferromagnetic dipole–dipole interaction between manganese ions with a Mn–Mn separation longer than 6.8873-(9) Å are negligible down to 4 K. By considering the magnetic behavior of **3**, the antiferromagnetic behavior of **2** is concluded to be due to the antiferromagnetic interaction between two manganese ions (15.397(2) Å separation) through TCNQ columns (···**BBCBB**···), where the anions are antiferromagnetically coupled to be diamangetic, and the exchange coupling constant (J) was estimated to be $-0.197(6)$ cm^{-1}. Crystal data: $[Mn^{II}(tpa)(\mu\text{-}O_2CCH_3)]_2(TCNQ)_2 \cdot 2CH_3CN$ (**1**), monoclinic, space group $P2_1/n$, $a = 18.798(6)$ Å, $b = 19.260(3)$ Å, $c = 8.973(2)$ Å, $\beta = 99.03(2)°$, $V = 3208(1)$ Å^3, $Z = 2$, and $R = 0.059$ ($R_w = 0.059$) for 4185 data with $|F_o| > 3\sigma(F_o)$; $[Mn^{II}(tpa)(TCNQ)(CH_3OH)](TCNQ)_2 \cdot CH_3CN$(**2**), triclinic, space group $P\bar{1}$, $a = 9.937(3)$ Å, $b = 31.608(4)$ Å, $c = 8.207(2)$ Å, $\alpha = 96.33(1)°$, $\beta = 92.91(2)°$, $\gamma = 89.19(2)°$, $V = 2559(1)$ Å^3, $Z = 2$, and $R = 0.045$ ($R_w = 0.058$) for 5074 data with $|F_o| > 6\sigma(F_o)$; $[Mn^{II}(tpa)(NCS)_2] \cdot CH_3CN$ (**3**), orthorhombic, space group $P2_12_12_1$, with $a = 13.271(2)$ Å, $b = 15.717(2)$ Å, $c = 11.800(2)$ Å, $V = 2461.2(5)$ Å^3, $Z = 4$, and $R = 0.037$ ($R_w = 0.042$) for 2380 data with $|F_o| > 6\sigma(F_o)$.

Introduction

Intense effort is currently concentrated on synthesis of new solids which exhibit a high electrical conductivity and magnetic ordering. In order to obtain such macroscopic properties, it is necessary to have a multidimensional network having a strong electronic interaction. Some organic anion radicals such as $TCNQ^-$ (tetracyanoquinodimethane), $TCNE^-$ (tetracyanoethylene),[1] and $DCNQI^-$ (dicyanoquinonediimine)[2] have been known to form a variety of stacks (network structure) due to intermolecular charge transfer interactions. If paramagnetic metal centers are assembled into the organic radical network, interesting magnetic or conductive properties might be obtained.

Metal complexes with TCNQ families including TCNE and DCNQI have been studied from the structural and magnetochemical view points. Among the organic radical compounds, TCNQ[3] is the most extensively studied system, and some inorganic salts have shown extremely high electric conductivity down to low temperature.[1] The first transition metal complex with TCNQ, $[M(abpt)_2(TCNQ)]$ (M = Cu, Ni, Co)[4] and $[Cu_2(L)(TCNQ)_2]$[5] (abpt = 3,5-bis(pyridin-2-yl)-4-amino-1,2,4-triazole and L = a tetra-bis(Schiff base) macrocycle resulting from the 2/2 condensation of 1,3-diaminopropane and 2,6-diformyl-4-methylphenol), have been prepared, and the magnetic studies for the copper complexes have shown no magnetic interaction between the paramagnetic centers due to the lack of overlap of the magnetic orbitals. On the other hand, reactions of TCNE with metal complexes lead to the formation of charge transfer complexes

† Department of Chemistry, Faculty of Science, Tohoku University.
‡ Institute for Materials Research, Tohoku University.
● Abstract published in *Advance ACS Abstracts,* November 1, 1993.

(1) Endres, H. In *Extended Linear Chain Compounds*; Miller, J. S., Ed.; Plenum Press: New York, 1983; Vol. 3, p 263.
(2) (a) Aumüller, A.; Erk, P.; Klebe, G.; Hünig, S.; von Schütz, J. U.; Werner, H. P. *Angew. Chem., Int. Ed. Engl.* **1986**, *25*, 740. (b) Mori, T.; Inokuchi, H.; Kobayashi, A.; Kato, R.; Kobayashi, H. *Phys. Rev. B* **1988**, *38*, 5913. (c) Kato, R.; Kobayashi, H.; Kobayashi, A. *J. Am. Chem. Soc.* **1989**, *111*, 5224.
(3) Acker, D. S.; Harder, R. J.; Mahler, W.; Melby, R. J.; Benson, R. E.; Mochel, W. E. *J. Am. Chem. Soc.* **1960**, *82*, 6408.
(4) Cornelissen, J. P.; van Diemen, J. H.; Groeneveld, L. R.; Haasnoot, J. G.; Spek, A. L.; Reedijk, J. *Inorg. Chem.* **1992**, *31*, 198.
(5) Lacroix, P.; Kahn, O.; Gleizes, A.; Valade, L.; Cassoux, P.; *Nouv. J. Chim.* **1984**, *8*, 643.

0020-1669/93/1332-5697$04.00/0

Table I. Crystallographic Data for $[Mn^{II}(tpa)(\mu\text{-}O_2CCH_3)]_2(TCNQ)_2\cdot 2CH_3CN$ (**1**) and $[Mn^{II}(tpa)(TCNQ)(CH_3OH)](TCNQ)_2\cdot CH_3CN$ (**2**), $[Mn^{II}(tpa)(NCS)_2]\cdot CH_3CN$ (**3**)

	1	**2**	**3**
formula	$C_{68}H_{56}Mn_2N_{18}O_4$	$C_{57}H_{37}MnN_{17}O_1$	$C_{22}H_{21}MnS_2N_7$
fw	1299.19	1030.97	502.51
temp (°C)	22	22	22
cryst syst	monoclinic	triclinic	orthorhombic
space group	$P2_1/n$	$P\bar{1}$	$P2_12_12_1$
a (Å)	18.798(6)	9.937(3)	13.271(2)
b (Å)	19.260(3)	31.608(4)	15.717(2)
c (Å)	8.973(2)	8.207(2)	11.800(2)
α (deg)	90.0	96.33 (1)	90.0
β (deg)	99.03(2)	92.91(2)	90.0
γ (deg)	90.0	89.19(2)	90.0
V (Å^3)	3208(1)	2559(1)	2461.2(5)
Z	2	2	4
D_{obs} (g cm^{-3})	1.340	1.332	1.358
D_{calc} (g cm^{-3})	1.345	1.338	1.356
radiation (Mo Kα) (Å)	0.710 69	0.710 69	0.710 69
μ(Mo Kα) (cm^{-1})	4.82	3.35	7.51
no. of tot. data collcd	4678	9027	3181
no. of indep data	4185 $\lvert F_o\rvert > 3\sigma(F_o)$	5074 $\lvert F_o\rvert > 6\sigma(F_o)$	2380 $\lvert F_o\rvert > 6\sigma(F_o)$
transm coeff	0.962–0.998	0.960–0.995	0.973–1.000
R^a	0.059	0.045	0.037
$R_w{}^b$	0.059	0.058	0.042

^{a} $R = \sum(|F_o|-|F_c|)/\sum|F_o|$. ^{b} $R_w = [\sum w(|F_o|-|F_c|)^2/\sum w|F_o|^2]^{1/2}$; $w = (\sigma_c^2 + (0.020|F|^2)^{-1}$ for **1**, $w = (\sigma_c^2 + (0.025|F|)^2)^{-1}$ for **2**, and w $(\sigma_c^2 + (0.020|F|)^2)^{-1}$ for **3**.

with a variety of bonding arrangements. [Mn(TPP)][TCNE][6] (TPP = *meso*-tetraphenylporphyrin) and $[M(hfacac)_2TCNE]$[7] (M = Co and Cu, and hfacac = hexafluoroacetylacetone) have been reported to have a linear chain structure in which TCNE bridges two metal centers in μ_2 fashion. Metallocene–TCNE charge transfer complexes have shown a nonbonded structure between them; however, the magnetic interactions between metal complexes and organic radicals in $[Fe(C_5Me_5)_2](TCNE)$[8] and $[V(TCNE)_x\cdot y(CH_2Cl_2)$[9] ($C_5Me_5$ = pentamethylcyclopentadiene) are strong enough to show magnetic ordering.

We have been concerned with control of the magnetic interaction in multinuclear and low-dimensional complexes. The dinuclear iron(III) complex $[Fe_2(bpmar)(H_2O)_4](NO_3)_4\cdot 3H_2O$ (H_2bpmar = 4,6-bis[(2′-pyridylmethyl)amino)methyl]-2-methylresorcinol) was designed to have a ferromagnetic interaction (J = 0.65 cm^{-1}) between the iron centers due to the topological network of dπ spins to the bridging ligand.[10] An oxalato-bridged copper(II) complex [Cu(bpy)(ox)] (bpy = bipyridine) with a one-dimensional structure showed an intrachain ferromagnetic interaction (J = 1.22(4) cm^{-1}) due to the orthogonal arrangement of the magnetic orbitals on the adjacent units.[11] The ferromagnetic interactions attained in the above complexes seem to be too weak to have macroscopic properties like a molecular-based ferromagnet even if the ferromagnetic interaction can be multidimensionally expanded. Some organic radicals have been known to form a multidimensional network with a strong electronic interaction. If paramagnetic metal complexes are incorporated into the radical network, such molecular assemblies might have interesting physical properties like molecular-based ferrimagnets or magnetic metals.

In this study, we aim to prepare the organic radical network having paramagnetic metal complexes as network components in which the incorporated metal complexes have magnetic interactions through radical network. In order to have magnetic interactions, magnetic orbitals of each molecule should direct at each other.[12] A manganese(II) ion in the high-spin state has five spins, where each d orbital has a spin. If organic radicals directly coordinate to the manganese ion, more than one of the d-orbitals can overlap with the magnetic orbital of the coordinated radicals through either a σ or a π pathway, or both. Hence, the manganese ions can have magnetic interaction with the organic radicals. We have synthesized manganese(II) complexes with TCNQ radical ions, and their crystal structures and magnetic properties have been studied in order to explore the nature of the magnetic interaction between metal centers and TCNQ radicals.

Table II. Positional and Equivalent Isotropic Displacement Coefficients (Å^2) for $[Mn^{II}(tpa)(\mu\text{-}O_2CCH_3)]_2(TCNQ)_2\cdot 2CH_3CN$ (**1**)

	x/a	y/b	z/c	U^a
Mn	0.496963(3)	0.58716(3)	0.61000(6)	0.0307(2)
N(1)	0.4311(2)	0.7014(2)	0.5703(3)	0.039(1)
N(2)	0.3710(2)	0.5802(2)	0.4346(3)	0.041(1)
N(3)	0.3794(2)	0.6005(2)	0.7573(4)	0.044(1)
N(4)	0.5549(2)	0.6529(2)	0.7409(3)	0.041(1)
N(5)	0.5968(2)	0.7804(2)	1.2403(4)	0.063(1)
N(6)	0.3703(2)	0.7694(2)	1.0610(4)	0.064(2)
N(7)	0.6460(2)	1.1104(2)	0.6503(5)	0.069(2)
N(8)	0.4145(2)	1.1041(2)	0.4896(4)	0.056(1)
C(1)	0.3869(2)	0.7055(2)	0.4193(5)	0.052(2)
C(2)	0.4963(2)	0.7451(2)	0.5827(5)	0.048(2)
C(3)	0.3893(3)	0.7207(2)	0.6914(5)	0.053(2)
C(4)	0.3445(2)	0.6407(2)	0.3747(4)	0.044(1)
C(5)	0.2810(2)	0.6417(3)	0.2713(5)	0.061(2)
C(6)	0.2459(2)	0.5807(3)	0.2295(6)	0.072(2)
C(7)	0.2732(2)	0.5192(3)	0.2903(5)	0.066(2)
C(8)	0.3359(2)	0.5212(2)	0.3903(5)	0.052(2)
C(9)	0.3457(2)	0.6617(2)	0.7392(4)	0.042(1)
C(10)	0.2760(2)	0.6709(2)	0.7695(5)	0.056(2)
C(11)	0.2416(2)	0.6156(3)	0.8228(6)	0.065(2)
C(12)	0.2755(3)	0.5528(3)	0.8430(6)	0.067(2)
C(13)	0.3438(3)	0.5474(3)	0.8066(5)	0.060(2)
C(14)	0.5528(2)	0.7212(2)	0.7093(4)	0.043(1)
C(15)	0.6027(3)	0.7670(2)	0.7867(5)	0.060(2)
C(16)	0.6553(3)	0.7417(3)	0.8953(5)	0.073(2)
C(17)	0.6591(3)	0.6727(3)	0.9267(5)	0.065(2)
C(18)	0.6075(2)	0.6293(2)	0.8476(5)	0.052(2)
C(19)	0.5647(2)	0.9232(2)	0.9687(4)	0.040(1)
C(20)	0.4986(2)	0.883(2)	0.9643(4)	0.037(1)
C(21)	0.4403(2)	0.9107(2)	0.8542(4)	0.040(1)
C(22)	0.4483(2)	0.9646(2)	0.7595(4)	0.040(1)
C(23)	0.5145(2)	1.0005(2)	0.7665(4)	0.035(1)
C(24)	0.5727(2)	0.9767(2)	0.8738(4)	0.036(1)
C(25)	0.4898(2)	0.8323(2)	1.0638(4)	0.040(1)
C(26)	0.4231(2)	0.7980(2)	1.0613(4)	0.045(1)
C(27)	0.5490(2)	0.8044(2)	1.1621(5)	0.044(1)
C(28)	0.5232(2)	1.0571(2)	0.6695(4)	0.038(1)
C(29)	0.4637(2)	1.0831(2)	0.5688(4)	0.040(1)
C(30)	0.5908(2)	1.0870(2)	0.6594(4)	0.044(1)
O(1)	0.5010(2)	0.4985(1)	0.7310(3)	0.051(1)
O(2)	0.5283(1)	0.5910(2)	0.4217(3)	0.052(1)
C(31)	0.4892(2)	0.4351(2)	0.7069(4)	0.040(1)
C(32)	0.4988(3)	0.3884(3)	0.8425(5)	0.073(2)
N(9)	0.7449(3)	0.6191(3)	0.2841(6)	0.109(2)
C(33)	0.6989(3)	0.6768(3)	0.5089(6)	0.080(2)
C(34)	0.7246(3)	0.6444(3)	0.3825(6)	0.070(2)

^{a} Equivalent isotropic U defined as one-third of the trace of the orthogonalized U_{ij} tensor.

Experimental Section

Materials. All chemicals (Wako Chemicals, LTD) were used as received without further purification. The ligand tpa was prepared by

(6) Miller, J. S.; Calabrese, J. C.; McLean, R. S.; Epstein, A. J. *Adv. Mater.* **1992**, *4*, 498.
(7) Bunn, A. G.; Carroll, P. J.; Wayland, B. B. *Inorg. Chem.* **1992**, *31*, 1297.
(8) (a) Miller, J. S.; Calabrese, J. S.; Rommelmann, H.; Chittipeddi, S. R.; Zhang, J. H.; Reiff, W. M.; Epstein, A. K. *J. Am. Chem. Soc.* **1987**, *109*, 769. (b) Miller, J. S.; Epstein, A. K.; Reiff, W. M.; Epstein, A. K. *Chem. Rev.* **1988**, *80*, 201.
(9) Manriquetz, J. Yee, G. T.; McLean, R. S.; Epstein, A. J.; Miller, J. S. *Science* **1991**, *252*, 1415.
(10) Oshio, H. *J. Chem. Soc., Chem. Commun.* **1991**, 240.
(11) Oshio, H.; Nagashima, U. *Inorg. Chem.* **1992**, *31*, 3295.
(12) Oshio, H. *Inorg. Chem.* **1993**, *32*, 4123.

Table III. Positional and Equivalent Isotropic Displacement Coefficients (Å²) for $[Mn^{II}(tpa)(TCNQ)(CH_3OH)](TCNQ)_2 \cdot CH_3CN$ (**2**)

	x/a	y/b	z/c	U[a]		x/a	y/b	z/c	U[a]
Mn	0.44386(7)	0.24385(2)	0.17135(7)	0.0444(2)	C(22)	0.6759(4)	0.4600(1)	0.5520(4)	0.036(1)
N(1)	0.4351(4)	0.30823(9)	0.0635(4)	0.048(1)	C(23)	0.6597(4)	0.5011(1)	0.6374(5)	0.037(1)
N(2)	0.2392(4)	0.2719(1)	0.2257(4)	0.053(1)	C(24)	0.6484(4)	0.5362(1)	0.5570(5)	0.038(1)
N(3)	0.6475(4)	0.2516(1)	0.0746(4)	0.056(1)	C(25)	0.6363(4)	0.5706(1)	0.2988(4)	0.038(1)
N(4)	0.3541(4)	0.2261(1)	–0.0804(4)	0.051(1)	C(26)	0.6875(4)	0.4234(1)	0.6365(5)	0.041(1)
N(5)	0.6199(4)	0.6466(1)	0.4397(4)	0.068(2)	C(27)	0.6376(4)	0.5679(1)	0.1259(5)	0.045(1)
N(6)	0.6407(4)	0.5664(1)	–0.0146(5)	0.064(2)	C(28)	0.6267(4)	0.6121(1)	0.3800(5)	0.046(1)
N(7)	0.7059(4)	0.4248(1)	0.9493(5)	0.060(1)	C(29)	0.6983(4)	0.3821(1)	0.5513(5)	0.053(2)
N(8)	0.7062(5)	0.3485(1)	0.4821(5)	0.083(2)	C(30)	0.6946(4)	0.4247(1)	0.8095(5)	0.043(1)
N(9)	0.7263(4)	1.1121(1)	1.0454(5)	0.079(2)	C(31)	0.6434(4)	1.0059(1)	0.8409(5)	0.038(1)
N(10)	0.7370(4)	1.0300(1)	1.4334(5)	0.071(2)	C(32)	0.6147(4)	0.9715(1)	0.7290(5)	0.036(1)
N(11)	0.5497(5)	0.8996(1)	0.3546(5)	0.074(2)	C(33)	0.5991(4)	0.9302(1)	0.7805(4)	0.034(1)
N(12)	0.5587(4)	0.81942(9)	0.7549(4)	0.052(1)	C(34)	0.6141(4)	0.9268(1)	0.9509(5)	0.038(1)
N(13)	0.9394(4)	0.6473(1)	0.1521(5)	0.074(2)	C(35)	0.6435(4)	0.9610(1)	1.0618(5)	0.038(1)
N(14)	0.9785(4)	0.5676(1)	0.5428(5)	0.063(2)	C(36)	0.6592(4)	1.0021(1)	1.0108(5)	0.036(1)
N(15)	1.0908(5)	0.1450(1)	0.1120(6)	0.087(2)	C(37)	0.6904(4)	1.0372(1)	1.1259(5)	0.041(1)
N(16)	1.0871(5)	0.0716(1)	0.5306(6)	0.084(2)	C(38)	0.5753(4)	0.8940(1)	0.6637(4)	0.039(1)
C(1)	0.3439(6)	0.3365(1)	0.1659(6)	0.064(2)	C(39)	0.7104(4)	1.0786(1)	1.0803(5)	0.050(2)
C(2)	0.5733(5)	0.3247(1)	0.0748(6)	0.059(2)	C(40)	0.7154(4)	1.0332(1)	1.2958(6)	0.049(2)
C(3)	0.3832(6)	0.3014(1)	–0.1089(5)	0.054(2)	C(41)	0.5615(4)	0.8970(1)	0.4922(5)	0.047(1)
C(4)	0.2247(5)	0.3139(1)	0.2156(5)	0.057(2)	C(42)	0.5660(4)	0.8529(1)	0.7136(4)	0.040(1)
C(5)	0.1093(7)	0.3360(2)	0.2584(6)	0.076(2)	C(43)	0.9825(4)	0.5400(1)	–0.0565(5)	0.044(1)
C(6)	0.0057(7)	0.3145(3)	0.3113(7)	0.092(3)	C(44)	0.9859(4)	0.5360(1)	0.1163(5)	0.041(1)
C(7)	0.0175(6)	0.2712(3)	0.3184(7)	0.086(3)	C(45)	0.9967(4)	0.5057(1)	–0.1678(5)	0.044(1)
C(8)	0.1343(6)	0.2506(2)	0.2731(6)	0.070(2)	C(46)	0.9719(4)	0.5712(1)	0.2298(5)	0.042(1)
C(9)	0.6727(5)	0.2898(1)	0.0247(5)	0.055(2)	C(47)	0.9530(4)	0.6134(1)	0.1848(5)	0.050(2)
C(10)	0.7848(6)	0.2976(2)	–0.0579(7)	0.071(2)	C(48)	0.9759(4)	0.5683(1)	0.4030(6)	0.046(1)
C(11)	0.8769(7)	0.2649(2)	–0.0918(8)	0.090(3)	C(49)	1.0143(4)	0.0387(1)	–0.0644(5)	0.049(2)
C(12)	0.8536(7)	0.2259(2)	–0.0413(8)	0.085(3)	C(50)	1.0318(4)	0.0366(1)	0.1109(5)	0.045(1)
C(13)	0.7388(6)	0.2201(2)	0.0412(7)	0.071(2)	C(51)	0.9842(4)	0.0042(1)	–0.1687(6)	0.047(2)
C(14)	0.3170(4)	0.2591(1)	–0.1618(5)	0.045(1)	C(52)	1.0600(4)	0.0723(1)	0.2173(6)	0.051(2)
C(15)	0.2275(5)	0.2545(2)	–0.2961(6)	0.066(2)	C(53)	1.0763(5)	0.1131(1)	0.1606(6)	0.061(2)
C(16)	0.1744(6)	0.2151(2)	–0.3477(6)	0.077(2)	C(54)	1.0756(5)	0.0715(1)	0.3893(7)	0.060(2)
C(17)	0.2144(6)	0.1807(2)	–0.2672(6)	0.075(2)	N(17)	0.8672(9)	0.1741(3)	0.459(1)	0.166(4)
C(18)	0.3020(5)	0.1880(2)	–0.1345(6)	0.066(2)	C(55)	0.7947(8)	0.1258(2)	0.6692(9)	0.123(3)
C(19)	0.6489(4)	0.5338(1)	0.3834(4)	0.035(1)	C(56)	0.8304(8)	0.1516(3)	0.555(1)	0.119(4)
C(20)	0.6658(4)	0.4928(1)	0.2980(5)	0.041(1)	C(57)	0.6041(6)	0.2506(2)	0.5229(7)	0.099(3)
C(21)	0.6787(4)	0.4576(1)	0.3780(5)	0.042(1)	O(1)	0.5089(4)	0.26973(9)	0.4221(4)	0.079(1)

[a] Equivalent isotropic U defined as one-third of the trace of the orthogonalized U_{ij} tensor.

the literature method.[13] LiTCNQ was prepared by adding a boiling solution of LiI (400 mg, 3 mmol) in 20 mL of acetonitrile to a boiling solution of TCNQ (408 mg, 2 mmol) in 200 mL of acetonitrile. A dark purple precipitate was collected by suction.

Preparations of $[Mn^{II}(tpa)(\mu\text{-}O_2CCH_3)]_2(TCNQ)_2 \cdot 2CH_3CN$ (1) and $[Mn^{II}(tpa)(TCNQ)(CH_3OH)](TCNQ)_2 \cdot CH_3CN$ (2). All procedures were carried out under a nitrogen atmosphere. Solvents were dried and degassed just before use. To a mixture of $Mn(CH_3COO)_2 \cdot 4H_2O$ (245 mg, 1 mmol) or $Mn(PF_6)_2 \cdot 4H_2O$ (417 mg, 1 mmol) and tpa (290 mg, 1 mmol) in acetonitrile (50 mL) was added LiTCNQ (422 mg, 2 mmol) in methanol (50 mL). After the mixture was allowed to stand overnight in a refrigerator, blue-black crystals resulted, which were filtered and washed with methanol. One of crystals was subjected to an X-ray structural analysis. Anal. Calcd for $C_{68}H_{56}Mn_2N_{18}O_4$ (**1**): C, 62.87; H, 4.34; N, 19.41 Found: C, 62.81; H, 4.31; N 19.24. Anal. Calcd for $C_{57}H_{37}MnN_{17}O$ (**2**): C, 66.41; H, 3.62; N 23.10 Found: C, 66.50; H, 3.52; N 23.08.

Preparation of $[Mn^{II}(tpa)(NCS)_2] \cdot CH_3CN$ (3). Na(NCS) (162 mg, 2mmol) in methanol was added to a methanol solution of $MnNO_3 \cdot 6H_2O$ (287 mg, 1 mmol) and tpa (290 mg, 1 mmol). The resulting pale green precipitate was filtered and washed with methanol. Recrystallization from acetonitrile gave a crystalline solid, which was subjected to an X-ray analysis. Anal. Calcd for $C_{22}H_{21}MnS_2N_7$ (**3**): C, 52.58; H, 4.21; N 19.51. Found: C, 52.63; H, 4.31; N 19.61.

Magnetic Measurement. Magnetic susceptibility data were collected in the temperature range 2.0–300 K and in an applied 1 k G field with the use of a Quantum Design Model MPMS SQUID magnetometer. Powdered samples were contained in the small half of a gelatin capsule and a phenolic guide (clear soda straw) was used to house the sample holder and was fixed to the end of the magnetometer drive rod. $[Cr(NH_3)_6](NO_3)_3$ was employed as duel magnetometer calibrants. Pascal's constants were used to determinate the constituent atom diamagnetism.[14]

X-ray Crystallography. Single crystals for **1** (0.45 × 0.35 × 0.30 mm³), **2** (0.50 × 0.43 × 0.20 mm³), and **3** (0.38 × 0.30 × 0.30 mm³) were individually mounted on glass fibers with epoxy resin. Diffraction data were collected on a Rigaku 7S four circle diffractometer with graphite-monochromatized Mo Kα radiation (λ = 0.710 69 Å). Empirical absorption corrections (ψ-scans) were carried out in each case. The lattice constants were optimized from a least-squares refinement of the settings of 25 carefully centered Bragg reflections in the range of $25° < 2\theta < 30°$. Crystallographic data were collected in Table I. The structures were solved by the direct method with SHELX-86[15] and Fourier techniques, and refined by the full-matrix least-squares method using XTAL 3.2.[16] All non-hydrogen atoms were readily located and refined with anisotropic thermal parameters and hydrogen atoms were located from difference Fourier maps and refined with isotropic thermal parameters. Final atomic parameters and equivalent isotropic thermal parameters for non-hydrogen atoms are listed in Tables II–IV.

Extended Hückel MO Calculation. The calculation was performed with a conventional program[17] written for a personal computer. Geometrical parameters were taken from the structural data.

Results and Discussion

Description of the Structure. $[Mn^{II}(tpa)(\mu\text{-}O_2CCH_3)]_2(TCNQ)_2 \cdot 2CH_3CN$ (1). An ORTEP drawing of the cation of **1** is depicted in Figure 1, and selected intramolecular bond distances and angles are listed in Table V. Complex **1** crystallizes in the monoclinic space group $P2_1/n$, and the cation is positioned on a

(13) Karlin, K. D.; Hayes, J. C.; Hutchinson, J. P.; Zubieta, J. *Inorg. Chem.* **1982**, *21*, 4106.

(14) *Theory and Application of Molecular Paramagnetism*; Boudreaux, E. A., Mulay, L. N. Eds.; Wiley and Sons, Inc.: New York, 1976.

(15) Sheldrick, G. M. *SHELX-86*; University of Göttingen: Göttingen, Germany, 1986.

(16) Hall, S. R.; Stewart, J. M. *XTAL3.2*; Universities of Western Australia and Maryland: Nedlands, Australia, and College Park, MD, 1992.

(17) (a) Hoffmann, R. *J. Chem. Phys.* **1963**, *39*, 1397. (b) Hoffman, R. Lipscomb, W. N. *J. Chem. Phys.* **1962**, *36*, 2179. (c) Howell, J.; Rossi, A.; Wallace, D.; Haraki, K.; Hoffmann, R. *QCPE* **1977**, No. 344.

Table IV. Positional and Equivalent Isotropic Displacement Coefficients (Å²) for $[Mn^{II}(tpa)(NCS)]_2 \cdot CH_3CN$ (**3**)

	x/a	*y/b*	*z/c*	*U*[a]
Mn	0.64557(4)	0.42928(4)	0.29378(5)	0.0387(2)
S(1)	1.0082(1)	0.4870(1)	0.3387(1)	0.0982(7)
S(2)	0.6732(1)	0.23096(9)	-0.0220(1)	0.0808(6)
N(1)	0.5824(3)	0.5083(2)	0.4440(3)	0.045(1)
N(2)	0.6229(2)	0.5624(2)	0.2249(3)	0.043(1)
N(3)	0.4708(2)	0.4384(2)	0.2619(3)	0.045(1)
N(4)	0.6420(3)	0.3413(2)	0.4443(3)	0.047(1)
N(5)	0.8028(3)	0.4576(3)	0.3280(3)	0.062(1)
N(6)	0.6599(3)	0.3470(3)	0.1534(3)	0.067(1)
N(7)	0.3780(4)	0.3315(4)	0.6239(5)	0.095(2)
C(1)	0.6131(4)	0.5969(3)	0.4246(4)	0.057(2)
C(2)	0.4722(3)	0.4986(3)	0.4504(4)	0.057(2)
C(3)	0.6280(4)	0.4740(3)	0.5482(3)	0.055(2)
C(4)	0.6162(3)	0.5829(3)	0.1146(3)	0.048(1)
C(5)	0.5958(4)	0.6638(3)	0.0778(4)	0.060(2)
C(6)	0.5802(4)	0.7260(3)	0.1569(5)	0.069(2)
C(7)	0.5815(4)	0.7055(3)	0.2716(4)	0.062(2)
C(8)	0.6051(3)	0.6226(2)	0.3018(4)	0.046(1)
C(9)	0.4274(4)	0.4243(3)	0.1612(4)	0.058(1)
C(10)	0.3339(4)	0.4549(4)	0.1342(5)	0.080(2)
C(11)	0.2823(4)	0.5030(5)	0.2126(7)	0.100(3)
C(12)	0.3282(4)	0.5200(4)	0.3139(5)	0.076(2)
C(13)	0.4221(3)	0.4861(3)	0.3372(4)	0.049(1)
C(14)	0.6533(4)	0.2574(3)	0.4416(4)	0.058(2)
C(15)	0.6597(4)	0.2075(3)	0.5382(5)	0.070(2)
C(16)	0.6538(4)	0.2464(4)	0.6409(4)	0.071(2)
C(17)	0.6417(4)	0.3329(3)	0.6467(4)	0.060(2)
C(18)	0.6364(3)	0.3791(3)	0.5475(3)	0.048(1)
C(19)	0.8884(3)	0.4697(3)	0.3331(4)	0.053(2)
C(20)	0.6646(3)	0.2986(3)	0.0808(4)	0.050(1)
C(21)	0.4165(5)	0.2534(5)	0.8152(6)	0.117(3)
C(22)	0.3946(4)	0.2979(4)	0.7088(7)	0.081(2)

[a] Equivalent isotropic *U* defined as one-third of the trace of the orthogonalized U_{ij} tensor.

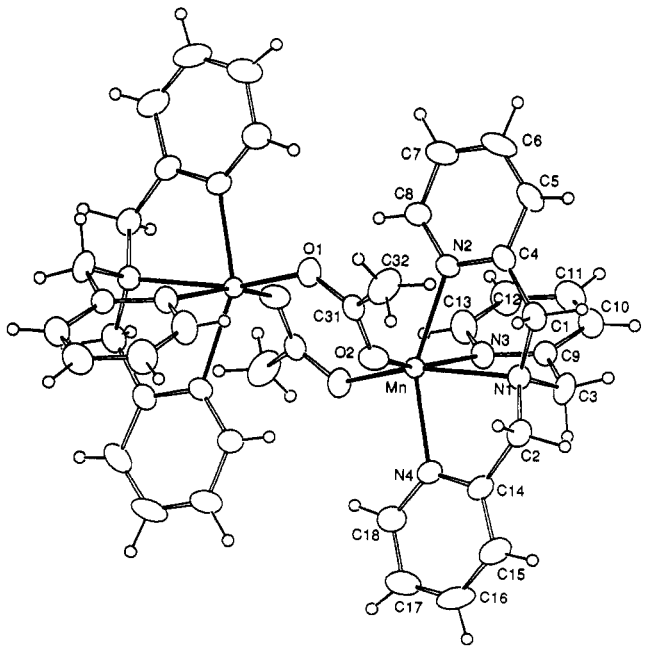

Figure 1. ORTEP drawing of the cation $[Mn^{II}(tpa)(\mu\text{-}O_2CCH_3)]_2^{2+}$ in **1**.

crystallographic inversion center. The asymmetric unit thus consists of half of the cation. Manganese ions in each asymmetric unit are bridged by the two acetates in syn–anti mode, that is, the syn lone pair on one carboxylate oxygen and the anti lone pair on the other. Iron(II) complexes $[Fe_2(TPA)_2(OAc)_2](BPh_4)_2$, in which the iron ion has similar coordination geometries to the manganese ion in **1**, were reported.[18] Six coordination sites of the manganese atom are completed by the four nitrogen and two oxygen atoms from tpa and bridging acetate ion, respectively. The Mn–N(amine) bond trans to the syn carboxylates oxygen

Table V. Selected Bond Lengths (Å) and Angles (deg) for $[Mn^{II}(tpa)(\mu\text{-}O_2CCH_3)]_2(TCNQ)_2 \cdot 2CH_3CN$ (**1**)

Mn–N(1)	2.326(3)	Mn–N(2)	2.239(3)
Mn–N(3)	2.323(4)	Mn–N(4)	2.227(3)
Mn–O(1)	2.060(3)	Mn–O(2)	2.160(3)
Mn–Mn	4.145(1)		
N(1)–Mn–N(2)	75.3(1)	N(1)–Mn–N(3)	75.2(1)
N(1)–Mn–N(4)	74.0(1)	N(1)–Mn–O(1)	157.1(1)
N(1)–Mn–O(2)	91.9(1)	N(2)–Mn–N(3)	79.0(1)
N(2)–Mn–N(4)	148.4(1)	N(2)–Mn–O(1)	117.2(1)
N(2)–Mn–O(2)	85.4(1)	N(3)–Mn–N(4)	99.6(1)
N(3)–Mn–O(1)	88.0(1)	N(3)–Mn–O(2)	161.8(1)
N(4)–Mn–O(1)	94.1(1)	N(4)–Mn–O(2)	88.8(1)
O(1)–Mn–O(2)	107.6(1)		

atom is the longest (2.326(3) Å) among the Mn–N bonds, and the Mn–N(pyridine) bond trans to the anti carboxylate oxygen is also long (2.323(4) Å) compared with the other Mn–N(pyridine) bonds. The syn-bound carboxylate oxygen atom exhibits a shorter bond (2.060(3) Å) than that for the anti (2.160(3) Å). The basicity of the syn carboxylate oxygen is higher than that of the anti,[19] and this may cause different bond distances between manganese and oxygen atoms. The syn–anti bridging mode affords a Mn–Mn distance of 4.145(1) Å. Series of carboxylato-bridged iron(II) dinuclear complexes have been prepared, and their crystal structures were studied. The iron–iron distances vary as the bridging modes vary; that is, the syn–anti mode[18] gives longer iron–iron distances (4.288 Å) than the syn–syn mode (3.3–3.6 Å),[20] while the anti–anti mode gives the longest iron–iron distance (6.625 (3) Å).[21] Acetato-bridged manganese(II) complexes $[Mn_2L_2(OAc)_2]^{2+}$ [22] (L = *N*,*N*′-dimethyl-*N*,*N*′-bis-(2-pyridylmethyl)ethane-1,2-diamine) and $[Mn_2(bpy)_4(OAc)_2]^{2+}$ [23] (bpy = bipyridine) with the same syn–anti bridging mode as **1** show similar Mn–Mn distances (4.30–4.58 Å).

TCNQ anions have been known to stack in a variety of modes,[1] that is, a ring–ring overlap (R–R), a ring-external bond overlap (R–B), and external bond–external bond overlap (B–B) modes. Figure 2 shows the arrangement of the anions in a view parallel and perpendicular to the aromatic ring plane. The TCNQ monoanions form a dimer structure with the typical R–R mode, and their mean planes at a close distance are 3.21–3.23 Å apart. The TCNQ dimers form one dimensional stacks in the B–B mode with an interplanar distance of 3.20–3.22 Å.

$[Mn^{II}(tpa)(TCNQ)(CH_3OH)](TCNQ)_2 \cdot CH_3CN$ (2). An ORTEP diagram of the cation and a packing diagram in the *ac*-plane for **2** are depicted in Figures 3 and 4, respectively, and the selected intramolecular bond distances and angles are listed in Table VI. The crystal consists of a cation and four kinds of crystallographically independent TCNQ anions, called **A**, **B**, **C**, and **D**, where **C** and **D** are located on the center of symmetry. The manganese ion is pseudooctahedrally coordinated by four N

(18) Ménage, S.; Zhang, Y.; Hendrich, M. P.; Que, L., Jr. *J. Am. Chem. Soc.* **1992**, *114*, 7786.
(19) (a) Li, Y.; Houk, K. N. *J. Am. Chem. Soc.* **1989**, *111*, 4505. (b) Todayoni, B. M.; Huff, J.; Rebek, J. *J. Am. Chem. Soc.* **1991**, *113*, 2247. (c) Cramer, K. D.; Zimmerman, S. C. *J. Am. Chem. Soc.* **1990**, *112*, 3680. (d) Allen, F. H.; Kirby, A. J. *J. Am. Chem. Soc.* **1991**, *113*, 8829.
(20) (a) Hartman, J. R.; Rardin, R. L.; Chaudhuri, P.; Pohl, K.; Wieghardt, K.; Nuber, B.; Weiss, J.; Papaefthymiou, G. C.; Frankel, R. B.; Lippard, S. J. *J. Am. Chem. Soc.* **1987**, *109*, 7387. (b) Tolman, W. B.; Liu, S.; Bentsen, J. G.; Lippard, S. J. *J. Am. Chem. Soc.* **1991**, *113*, 152. (c) Rardin, R. L.; Poganiuch, P.; Bino, A.; Goldberg, D. P.; Tolman, W. B.; Liu, S.; Lippard, S. J. *J. Am. Chem. Soc.* **1992**, *114*, 5240. (d) Borovik, A. S.; Que, L., Jr. *J. Am. Chem. Soc.* **1988**, *110*, 2345. (e) Borovik, A. S.; Hendrich, M. P.; Holman, T. R.; Münck, E.; Papaefthymiou, V.; Que, L., Jr. *J. Am. Chem. Soc.* **1990**, *112*, 6031. (f) Ménage, S.; Brennan, B. A.; Juarez-Garcia, C.; Münck, E.; Que, L., Jr. *J. Am. Chem. Soc.* **1990**, *112*, 6423.
(21) Martinez-Lorente, M. A.; Tuchagues, J. P.; Pétrouléas, V.; Savariault, J. M.; Poinsot, R.; Drillon, M. *Inorg. Chem.* **1991**, *30*, 3587.
(22) Che, C.-M.; Tang, W. T.; Wong, K. Y.; Wong, W. T.; Lai, T. F. *J. Chem. Res., Synop.* **1991**, 30.
(23) Rardin, R. L.; Tolman, W. B.; Lippard, S. J. *New J. Chem.* **1991**, *15*, 417.

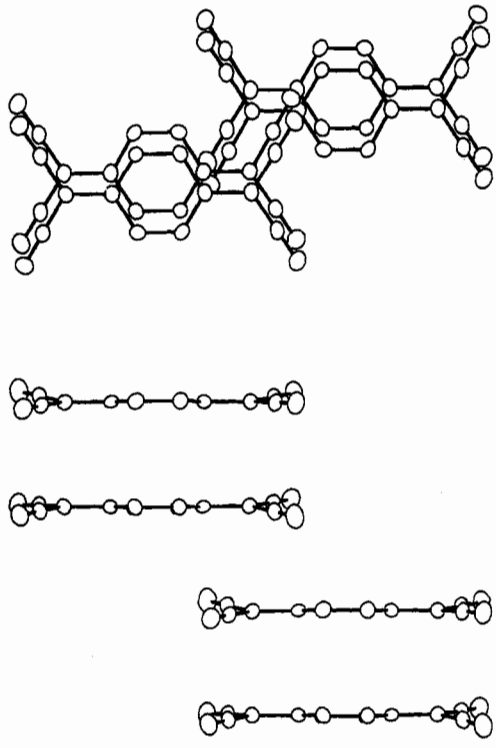

Figure 2. Arrangement of $TCNQ^-$ ion in $[Mn^{II}(tpa)(\mu\text{-}O_2CCH_3)]_2(TCNQ)_2\cdot 2CH_3CN$ (**1**).

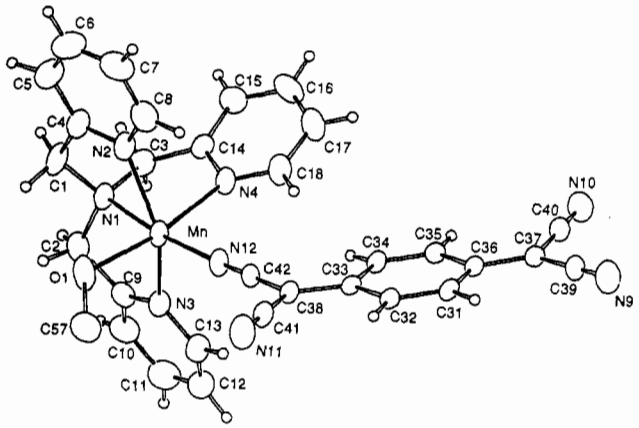

Figure 3. ORTEP drawing of $[Mn^{II}(tpa)(TCNQ)(CH_3OH)]^{n+}$ in **2**.

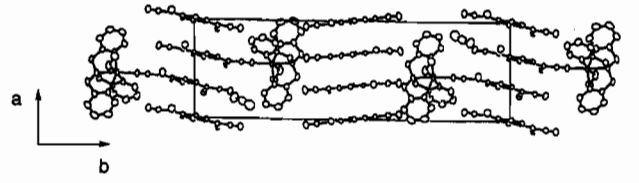

Figure 4. Projection view on *ac* plane of $[Mn^{II}(tpa)(TCNQ)(CH_3OH)]\cdot(TCNQ)_2\cdot CH_3CN$.

atoms, one N atom, and one O atom from tpa, TCNQ (the anion **B**), and CH_3OH, respectively. The tripod ligand tpa forms a characteristic configuration to accommodate the five membered chelate ring. Average N(amine)–Mn–N(pyridine) bond angles are about 75° and the Mn–N(amine) bond is longer (2.306(3) Å) than other Mn–N(pyridine) bonds (2.225(3)–2.253(4) Å). It should be noted that the Mn–N(TCNQ) bond, which is trans to Mn–N(amine), is the shortest (2.153(3) Å) among the Mn–N bonds. TCNQ anions stack with a different stacking mode (Figure 5) and form columns (Figure 4). Two **A**'s form a dimeric unit (**AA**) with the R–R mode, and **AA** and **C** are alternately aligned to form a column (···**AACAA**···) (Figure 4), where the stacking mode between **A** and **C** is the B–B mode. Intermolecular **B** units form eclipsed dimers (**BB**) in the R–R mode and the dimers form

Table VI. Selected Bond Lengths (Å) and Angles (deg) for $[Mn^{II}(tpa)(TCNQ)(CH_3OH)](TCNQ)_2\cdot CH_3CN$ (**2**)

Mn–N(1)	2.306(3)	Mn–N(2)	2.253(4)
Mn–N(3)	2.237(4)	Mn–N(4)	2.225(3)
Mn–N(12)	2.153(3)	Mn–O(1)	2.198(3)
Mn–Mn[a]	15.397(2)		
N(1)–Mn–N(2)	74.1(1)	N(1)–Mn–N(3)	74.6(1)
N(1)–Mn–N(4)	77.6(1)	N(1)–Mn–N(12)	173.3(1)
N(1)–Mn–O(1)	96.1(1)	N(2)–Mn–N(3)	148.4(1)
N(2)–Mn–N(4)	85.0(1)	N(2)–Mn–N(12)	105.5(1)
N(2)–Mn–O(1)	86.9(1)	N(3)–Mn–N(4)	91.6(1)
N(3)–Mn–N(12)	106.1(1)	N(3)–Mn–O(1)	93.1(1)
N(4)–Mn–N(12)	95.7(1)	N(4)–Mn–O(1)	170.8(1)
N(12)–Mn–O(1)	90.5(1)		

[a] Key to symmetry operation: $1-x, -y, -z$.

a column (···**BBDBB**···) with **D**, where **BB** stacks with **D** (Figure 4) in the R–B mode. $[Mn^{II}(tpa)(CH_3OH)]$ units are directly bound by the anion **B**, and two manganese atoms are thus connected through the dimer **BB** with a Mn–Mn separation of 15.397(2) Å. As a result, the manganese complex is incorporated into ···**BBDBB**··· column. On the other hand, the symmetry translation of the Mn atom along the *a*-axis gives the closest Mn–Mn distance of 8.207(2) Å.

It is important to know the electronic states of the each anion in order to interpret the magnetic behavior of the compounds. Intramolecular bond distances of the TCNQ anion reflect the electronic structure of the molecule. Figure 6 shows the LUMO of the TCNQ which was calculated by the extended Hückel molecular orbital method. Bonds with an antibonding character like **a** and **c** (see Figure 6) should be lengthen as the negative charge of the molecule increased, while bonds with a bonding character like **b** and **d** should be reversed. Interatomic bond lengths for **A** and **C** show the same values as **B** and **D**, respectively, this leads to conclude that the formal charges of **A** and **C** are the same as those of **B** and **D**, respectively. The cation $[Mn(tpa)(CH_3OH)]$ is diionic so the two negative charges are equivalently shared with **AC** and **BD** pairs; that is, the TCNQ ions are mixed valent. Intramolecular bond lengths of the TCNQ anions in **1** and **2** are listed together in Table VII. Bonds **a** (1.352–1.368 Å) and **c** (1.404–1.425 Å) for **A** and **B** are longer than those (1.336–1.350 and 1.372–1.380 Å) for **C** and **D**, respectively, while bonds **b** (1.413–1.427 Å) and **d** (1.408–1.423 Å) for **A** and **B** are shorter than those (1.432–1.449 and 1.415–1.433 Å) for **C** and **D**, respectively. Hence, **A** and **B** are concluded to be more negative than **C** and **D**. The TCNQ monoanion in **1** shows longer **a** and **c** bonds (Table VII).

$[Mn^{II}(tpa)(NCS)_2]\cdot CH_3CN$ (3). The structure is noncentrosymmetric. The noncentrosymmetric structure and its inversion were refined using the complete data set of all observed reflections and 289 variable parameters. The final R/R_w values for the structure presented here were calculated to be 0.037/0.042, and those for its inversion, to be 0.039/0.045. Final positional and equivalent isotropic displacement parameters are given in Table IV. An ORTEP drawing of the molecule is depicted in Figure 7 and selected intramolecular bond lengths and angles are listed in Table VIII. A coordination geometry about the manganese atom can be expressed as a pseudooctahedron which is completed by four nitrogen atoms from tpa and two from NCS anions. Mn–N(NCS) bonds (2.110(4) Å and 2.171(4) Å) show shorter lengths than Mn–N(tpa) bonds (2.252–2.354 Å). Mn–N(amine) (2.321(3) Å) has rather long bond length compared with two of the Mn–N(pyridine) bonds. The Mn–N(pyridine) bond, which is trans to the NCS^-, is lengthened compared with the other Mn–N(pyridine) bonds due to a trans effect of the NCS anions.

The tripodal ligand tpa causes a characteristic coordination geometry in metal complexes. The bonds between Mn and N(tpa) atoms in **3** (2.252–2.354 Å) are almost the same as those of **2** (2.225–2.306 Å). The average N(amine)–Mn–N(pyridine) bond

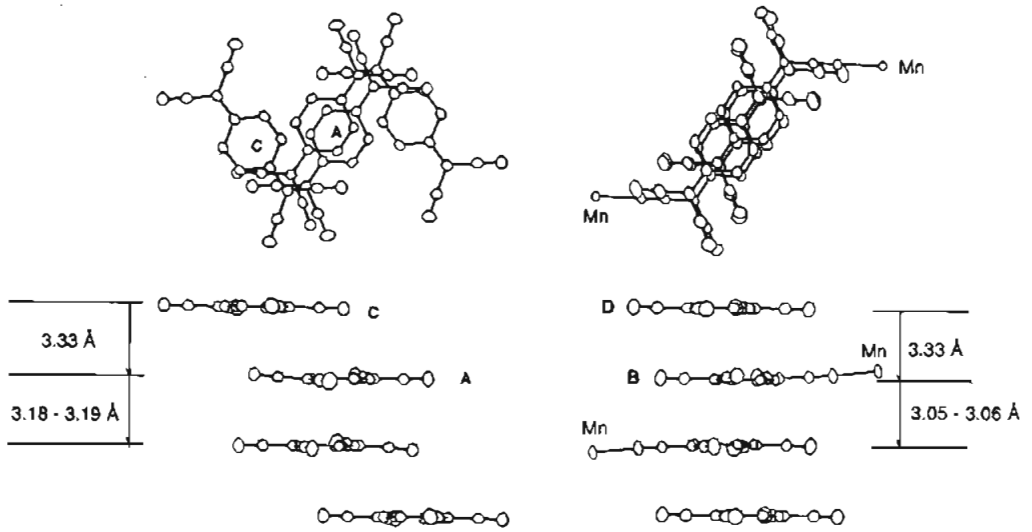

Figure 5. Stacking diagram of TCNQ anions in $[Mn^{II}(tpa)(TCNQ)(CH_3OH)](TCNQ)_2 \cdot CH_3CN$ (**2**).

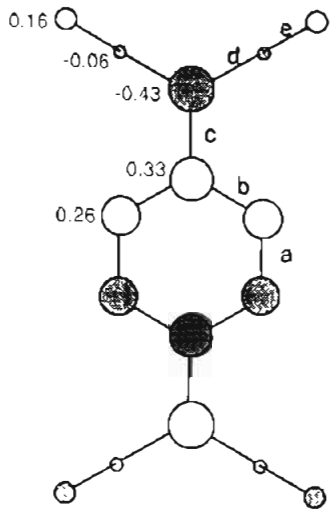

Figure 6. EHMO diagram of the LUMO of TCNQ. Numerals represent orbital coefficients, and **a**, **b**, **c**, and **d** represent the bond notations used in the text.

Table VII. Intramolecular Bond Distances (Å) for TCNQ Anions[a] in $[Mn^{II}(tpa)(\mu\text{-}O_2CCH_3)]_2(TCNQ)_2 \cdot 2CH_3CN$ (**1**) and $[Mn^{II}(tpa)(TCNQ)(CH_3OH)](TCNQ)_2 \cdot CH_3CN$ (**2**)

	bond a	bond b	bond c	bond d	bond e
[TCNQ]⁻ in **1**	1.361(5)	1.406(6)	1.427(5)	1.414(6)	1.148(5)
	1.364(6)	1.423(5)	1.420(5)	1.412(5)	1.135(6)
		1.418(5)		1.415(5)	1.146(6)
		1.414(5)		1.411(6)	1.148(5)
TCNQ A in **2**	1.354(6)	1.415(5)	1.419(5)	1.413(6)	1.147(5)
	1.352(5)	1.419(5)	1.413(5)	1.410(5)	1.151(6)
		1.423(5)		1.418(5)	1.147(6)
		1.418(5)		1.415(6)	1.150(5)
TCNQ B in **2**	1.368(5)	1.413(5)	1.425(4)	1.418(5)	1.142(6)
	1.358(5)	1.427(5)	1.404(5)	1.423(6)	1.154(6)
		1.415(5)		1.420(6)	1.141(6)
		1.422(5)		1.408(5)	1.152(5)
TCNQ C in **2**	1.350(5)	1.437(6)	1.380(5)	1.430(6)	1.138(6)
		1.432(6)		1.433(6)	1.150(6)
TCNQ D in **2**	1.336(6)	1.449(6)	1.372(5)	1.433(6)	1.139(6)
		1.436(6)		1.415(7)	1.159(7)

[a] Bond notations are described in Figure 6.

angle in **3** is about 74.2°, where the corresponding angle in **2** is 75.4°. The Mn–N(NCS) bond shows the same length as Mn–O(CH_3OH) (2.198(3) Å) and Mn–N(TCNQ) (2.153(3) Å) in **2**. The bond angles N(amine)–Mn–N(NCS) in **3** and N(amine)–Mn–N(TCNQ) in **2** are 163.7(1) and 173.3(1)°, respectively. The coordination geometry of **3** can be regarded as being same

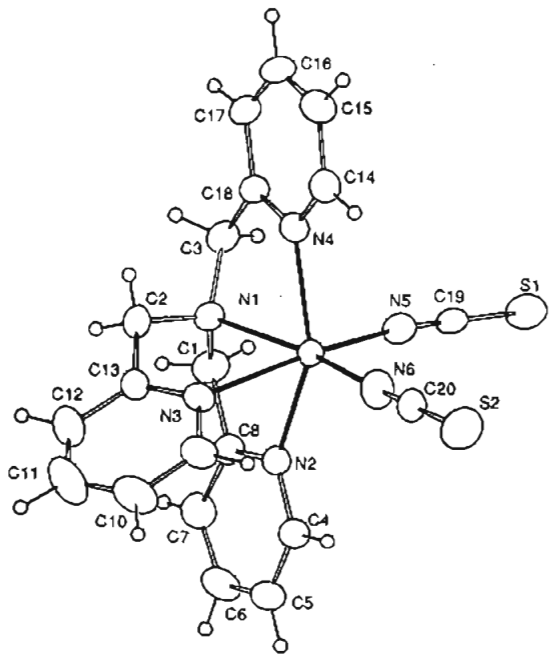

Figure 7. ORTEP drawing of $[Mn^{II}(tpa)(NCS)_2]$.

Table VIII. Selected Bond Lengths (Å) and Angles (deg) for $[Mn^{II}(tpa)(NCS)_2] \cdot CH_3CN$ (**3**)

Mn–N(1)	2.321(3)	Mn–N(2)	2.265(3)
Mn–N(3)	2.354(3)	Mn–N(4)	2.252(3)
Mn–N(5)	2.171(4)	Mn–N(6)	2.110(4)
Mn–Mn	6.8873(9)		
N(1)–Mn–N(2)	74.4(1)	N(1)–Mn–N(3)	74.5(1)
N(1)–Mn–N(4)	73.7(1)	N(1)–Mn–N(5)	95.5(1)
N(1)–Mn–N(6)	163.7(1)	N(2)–Mn–N(3)	75.8(1)
N(2)–Mn–N(4)	148.0(1)	N(2)–Mn–N(5)	90.3(1)
N(2)–Mn–N(6)	107.2(1)	N(3)–Mn–N(4)	98.2(1)
N(3)–Mn–N(5)	164.6(1)	N(3)–Mn–N(6)	90.0(1)
N(4)–Mn–N(5)	90.0(1)	N(4)–Mn–N(6)	104.2(1)
N(5)–Mn–N(6)	100.7(2)		

as that of **2**. It should be noted that the closest Mn–Mn distance in **3** is 6.8873(9) Å.

Magnetic Properties. Temperature dependent magnetic susceptibilities for **1**, **2**, and **3** have been measured down to 2.0 K, and $\chi_m T$ values are plotted vs. temperature (Figure 8), where χ_m is the molar magnetic susceptibility.

The $\chi_m T$ value (Figure 8a) of **1** decreases from 8.52 emu mol^{-1} K at 300 K to 0.63 emu mol^{-1} K at 2 K. There are two kinds of paramagnetic species in **1**, that is, the acetato-bridged

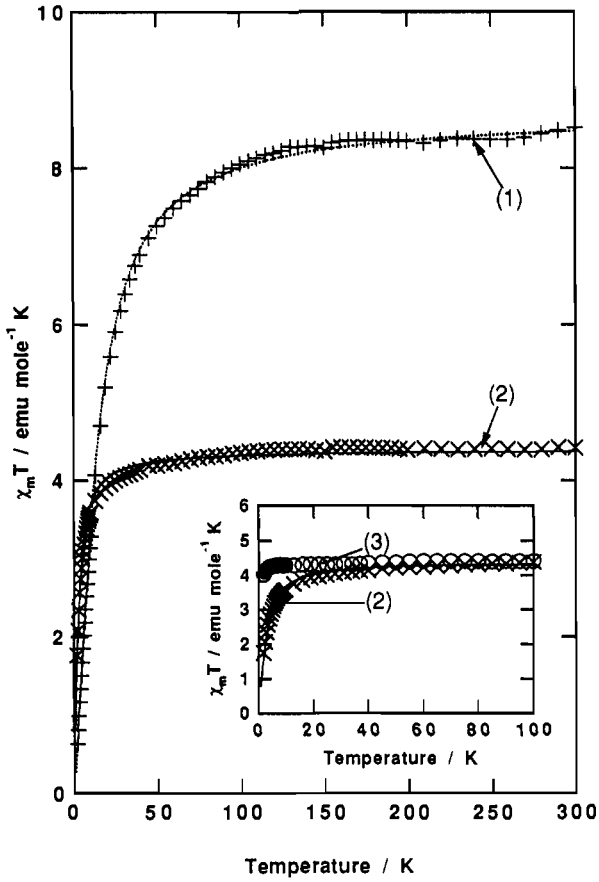

Figure 8. Temperature dependence of $\chi_m T$ for (+) $[Mn^{II}(tpa)(\mu\text{-}O_2CCH_3)]_2(TCNQ)_2\cdot 2CH_3CN$ (**1**), (×) $[Mn^{II}(tpa)(TCNQ)(CH_3OH)](TCNQ)_2\cdot CH_3CN$ (**2**), and (○) $[Mn^{II}(tpa)(NCS)_2]\cdot CH_3CN$ (**3**). Solid lines result from a least-squares fit using the parameters and equations described in the text.

manganese dimer and TCNQ dimer. The $\chi_m T$ value at 300 K is close to the spin-only value (8.757 emu mol^{-1} K) for the noninteracting manganese dimer ($S = {}^5/_2 \times 2$). The antiferromagnetic interaction between TCNQ dimer is supposed to be strong enough to be diamagnetic at 300 K. Therefore, it is reasonable to analyze the magnetic susceptibility data for the manganese dimer without the contribution of the TCNQ dimers. Assuming isotropic exchange, the exchange Hamiltonians is $H = -2JS_1\cdot S_2$ with $S_1 = S_2 = {}^5/_2$, and the magnetic susceptibility per mole of the dimer is given by[24]

$$\chi_m T = \frac{2Ng^2\beta^2}{k}\left[\frac{55 + 30x^{10} + 14x^{18} + 5x^{24} + x^{28}}{11 + 9x^{10} + 7x^{18} + 5x^{24} + 3x^{28} + x^{30}}\right] \quad (1)$$

where N, g, β, k, x are the Avogardro's number, g factor, Bohr magneton, and Boltzman constant, and $x = \exp(-J/kt)$, respectively, and J is the exchange coupling constant for the manganese dimer. The best fit parameters are found to be $g = 1.995(1)$ and $J = -0.972(6)$ cm^{-1}. The antiferromagnetic interaction of **1** is the same order as that ($J = -1.7$ cm^{-1}) of a carboxylato-bridged manganese(II) dimer reported for $[Mn^{II}_2(bpy)_2(C_3F_7COO)_4]$.[25]

The $\chi_m T$ vs. temperature plot (Figure 8b) for **2** shows a typical behavior for the paramagnetic species with an weak antiferromagnetic interaction, that is, the $\chi_m T$ values decrease as the temperature decreases starting from 120 K (4.39 emu mol^{-1} K) down to 2.0 K (1.76 emu mol^{-1} K), while the $\chi_m T$ values do not show a significant change (4.40 emu mol^{-1} K) above 120 K. The high-temperature values for $\chi_m T$ (4.40 emu mol^{-1} K) are almost the same as the spin-only value for the $S = {}^5/_2$ state (4.38 emu mol^{-1}). It is concluded that the observed magnetism for **2** results only from the manganese ion and the antiferromagnetic interactions between the TCNQ anions are of sufficient magnitude to render the dimers (or columns) diamagnetic. The decrease of $\chi_m T$ values as the temperature decreased can be accounted for by three factors: (i) an antiferromagnetic interaction between the manganese atoms through TCNQ column (σ or π pathway), where the Mn–Mn separation is 15.397 (2) Å; (ii) an antiferromagnetic dipole–dipole interaction between manganese atoms (the closest Mn–Mn separation is 8.207(2) Å); (iii) a zero-field splitting (ZFS) of the manganese ion. The ZFS in Mn^{2+} ion ($S = {}^5/_2$) does not affect the magnetic susceptibility down to very low temperatures because the ZFS for the Mn^{2+} ion is usually very small (of the order of 10^{-2} cm^{-1}) due to its electronic configuration ($^6A_1$) and the ground state is well-isolated from the higher energy level.[26] To address the origin of magnetic behavior of **2**, a mononuclear manganese(II) complex, $[Mn(tpa)(NCS)_2]\cdot CH_3CN$ (**3**), in which the closest Mn–Mn distance is 6.8873(9) Å and the coordination geometry about the manganese ion is similar to **2**, was prepared and the magnetic properties were studied. $\chi_m T$ values of **3** do not change down to 4 K followed by a decrease (Figure 8c) due to factor ii or factor iii. The contributions of the antiferromagnetic dipole–dipole interaction between manganese ions with a Mn–Mn separation longer than 6.8873 Å and zero-field splitting for the Mn^{2+} ion to the $\chi_m T$ are negligible down to 4 K. It is concluded that the decrease of $\chi_m T$ values for **2** starting from 120 K is due to the antiferromagnetic interaction between the manganese ions through TCNQ column (σ or π pathway, or both). The magnetic susceptibility for **2** was analyzed by the Van Vleck equation as in formula 1. A least-squares fit of the magnetic susceptibility equation to the data yielded $J = -0.197(6)$ cm^{-1} and $g = 2.003(1)$, and the solid line shown in Figure 8b was generated with these best-fit parameters. The estimated g values are very close to the value for a free electron, and this result supports the conclusion that the spin–orbit coupling and ZFS are negligible for **3**.

Conclusion

In $[Mn_2(tpa)_2(\mu\text{-}O_2CCH_3)_2](TCNQ)_2\cdot 2CH_3CN$ (**1**), the manganese ions were bridged by the acetate ions and no room for the coordination of TCNQ remained. No magnetic interactions between manganese ion and TCNQ anion were observed because of the lack of coordination of TCNQ to the manganese ion. In $[Mn(tpa)(TCNQ)(CH_3OH)](TCNQ)_2\cdot CH_3CN$ (**2**), one of the TCNQ ions, which forms a column structure, directly coordinates to the metal ion, and the manganese complex was successfully assembled into the organic radical network. Magnetic susceptibility measurements for **2** and mononuclear manganese(II) complex $[Mn(tpa)(NCS)_2](CH_3CN)$ (**3**) lead us to conclude that the manganese ions are antiferromagnetically coupled ($J = -0.197(6)$ cm^{-1}) through the TCNQ column, where the Mn–Mn separation is 15.397(2) Å. That is, the superexchange mechanism operates through the σ- or π-orbitals of the TCNQ column in **2**.

Acknowledgment. This work was in part supported by a Grant-in-Aid for Scientific Research on Priority Area "Molecular Magnetism" (Area No. 228/No. 05226203) and Grant No. 05453039 from Ministry of Education, Science and Culture, Japan.

Supplementary Material Available: Tables SI–SXV, listing X-ray data collection parameters, derived hydrogen positions, thermal parameters, bond distances, and angles, Figures SI, showing an ORTEP diagram of the TCNQ monoanion in **1**, and Figure SII, showing the bond lengths of the TCNQ anion in **2** (19 pages). Ordering information is given on any current masthead page.

(24) Hatfield, W. E. In *The Theory and Applications of Molecular Paramagnetism*; Boudreaus, E. A., Mulay, L. N., Eds.; John Wiley & Sons, Inc.: New York, 1976; Chapter 7.
(25) Wieghardt, K.; Bössek, U.; Nuber, B.; Weiss, J.; Bonvoisin, J.; Corbella, M.; Vitols, S. E.; Girerd, J. J. *J. Am. Chem. Soc.* **1988**, *110*, 7398.
(26) Carlin, R. L. *Magnetochemistry*; Springer-Verlag: Berlin, 1986; Chapter 4, p 64.